Original scientific paper

Anodic HfO$_2$ crossbar arrays for hydroxide-based memristive sensing in liquids

Ivana Zrinski[1,✉], Dominik Knapic[1], Achim Walter Hassel,[1,2] and Andrei Ionut Mardare[1,✉]

[1]*Institute of Chemical Technology of Inorganic Materials, Johannes Kepler University Linz, Altenberger Str. 69, 4040 Linz, Austria*

[2]*Danube Private University, Steiner Landstrasse 124, 3500 Krems-Stein, Austria*

Corresponding authors: ✉*ivana.zrinski@jku.at;* ✉*andrei.mardare@jku.at*

Abstract

The development of miniaturized and portable sensing devices is crucial to meeting the high processing capacity demands of contemporary computing systems. Hence, the conceptualization of memristive sensors for hydroxide-containing liquids is proposed in this study. Metal-insulator-metal (MIM) structures were formed on electrochemically anodized Hf thin films with Pt patterned as top electrodes. These MIM memristive structures were integrated into a crossbar array, allowing the investigation of a high number of potential memristor sensors. The MIM structures have demonstrated sensing possibilities in the detection of the hydroxyl ion in D-glucose, used as a standard solution. The sensing method was based on the resistive state ratio extracted from I-U sweeps measurements. Analytical characterization of the memristor sensor was done based on the resistive state ratio in relation to different concentrations of a standard solution drop cast directly on the surface of the device. Linearity was found for D-glucose concentrations ranging from 10 mM to 80 mM with a reasonable corresponding correlation factor (R^2=0.96809). Additionally, D-glucose incorporation in anodic oxide was studied by XPS to investigate its effect on conductive filaments formation. A carbon bonded by a single covalent bond to oxygen (O-C-O) was detected, confirming the proposed sensing mechanism defined by the glucose penetrating the oxide/electrode interface.

Keywords

Memristors, anodic oxides, ultra-thin films, liquid detection, valve metals

Introduction

Enormous progress has been recently made in the field of complementary metal-oxide-semiconductor (CMOS) technology [1-3]. With this respect, computing performance has leveled up with a demand for a large amount of data to be processed and stored. However, these computing systems rely on von Neuman architectures based on separated processing and memory units [1,3,4].

This architecture is inefficient in the sense that it considerably increases energy losses and limits processing speeds and scalability, thus defining an issue known as the von Neuman bottleneck. Clearly, a necessity for the development of miniaturized in-memory computing systems has emerged. As such, memristors are foreseen as an ideal replacement for conventional memories, being a nonvolatile type of memory [2,3]. Furthermore, not only that memristors can be used as ReRAMs, for neuromorphic networks, artificial synapses and image processing, but also in sensing applications [5-11].

The storage concept, based on the resistive switching between a high resistive state (HRS) and a low resistance state (LRS), can also be considered a sensing mechanism [12]. While describing the memory window and power consumption of memristors, the resistive state ratio (HRS/LRS) can also define sensing capacity. Following the same analogy, the larger the resistive state ratio, the larger the sensing capability of the device [6].

Additionally, memristors can be integrated into crossbar arrays due to their simple two-terminal structures, which can further increase their surface density [13-15]. At the same time, miniaturized sensing electronics are more desired than large conventional sensors that can be only utilized as separated units in computing systems [7].

Valve metals have already demonstrated promising memristive behavior [16-22]. One commonly used memory storage material in memristive devices is hafnium dioxide (HfO₂) [18-21]. Besides its wide band gap, high refractive index, high melting point, and high chemical stability, it is also used as a high-κ gate dielectric in the semiconductor industry [23-27,27,28]. Hence, there is a strong motivation for HfO₂ to be used as a sensing material. Until now, several gas or liquid sensors based on HfO₂ have been investigated [7,29-31]. However, the sensing mechanism in memory applications still requires further investigation. Memristive sensors have been studied for biomolecule detection or temperature probing in dry conditions [32-34]. Furthermore, the development of devices for liquids with hydroxyl group sensing is vital due to the wide range of their possible biomedical applications [6,7,31].

Finally, a sensing mechanism based on HfO₂ anodic memristors has been demonstrated in the current work for several *D*-glucose concentrations, which was used as a standard. Such sensing device has shown improved performance with respect to memristive-based sensors reported in the literature.

Experimental

Fabrication of memristors integrated into a crossbar array

The bottom electrodes of metal-insulator-metal (MIM) structured devices were produced by deposition by sputtering. The process was carried out in a high vacuum system with a base pressure in the range of 10^{-6} Pa. The deposition of Hf thin films onto pre-oxidized Si wafers was conducted in Ar atmosphere ($5 \cdot 10^{-1}$ Pa, 25° C) by applying a constant power to a high purity Hf target (99.95 % Demaco, The Netherlands) [35,36]. The Hf thin film was deposited through a pre-attached Ni shadow mask (Mecachimique, Pierrelaye, France). This allowed patterning parallel Hf lines, defining word lines or bottom electrodes (Figure 1a). Following that, these Hf metallic lines were used as working electrodes during the electrochemical oxidation process in a classical three-electrode set containing Hg/Hg₂SO₄/sat. K₂SO₄ electrode (0 V *vs.* Hg/Hg₂SO₄ = 0.640 V *vs.* SHE) as a reference electrode, and a commercial graphite foil, used as a counter electrode (0.5 mm thick, 99.8 % ThermoFisher, Erlangen, Germany). The resulting anodic oxide was grown potentiodynamically up to 8 V *vs.* SHE in 1 M phosphate buffer solution (PB), pH 7.0 (Na₂HPO₄, NaH₂PO₄, Merck, Darmstadt, Germany) [37]. Finally, Pt was also patterned through a pre-attached shadow mask in order to form

I. Zrinski *et al.*

J. Electrochem. Sci. Eng. **13(5)** (2023) 805-815

bit lines or top electrodes perpendicular to the bottom electrodes (Figure 1a). In this way, two terminal MIM structures are created at the intersections of the electrode lines, representing memristors as shown in Figures 1b, 1c and 1d.

Electrical measurements

Electrical measurements referring to *I-U* sweeps, endurance and retention evaluation were performed in environmental conditions (22 °C, 55 % relative humidity) using a self-developed electrical setup. A Gantry robot with XYZ stages, microscope cameras and force sensing is described in previous studies. The system is connected to Keithley 2450 SourceMeter Unit parameter analyzer and controlled via LabView software [35,36]. Pure Hf bottom electrodes were biased during *I-U* sweeping, while Pt top electrode remained grounded during the measurements. Electric contacts were established by contacting gold and stainless steel needles at the ends of metallic lines, thus the bottom and top electrodes, respectively. The contact force was controlled by a force sensor keeping it constant at 20±2 mN. Hence, direct needle contact on top of each MIM structure was avoided. This prevents the system from possible chemical reactions with the needle, mechanical damage such as breaking the thin film or any other undesirable effects. Once the switching voltages were determined, the pulsed voltage stress (PVS) method was applied for device lifetime testing (endurance measurements) at a maximum of 260 Hz. The resistance values were read at very low voltage values (20 mV), as in the case of retention measurements. In this case, devices were not switched from HRS to LRS state or vice versa, but HRS or LRS values were only read to test data retention.

Sensing characterization

In order to test the sensing response of memristors, different concentrations of *D*-glucose were drop cast on the surface of a device. Phosphate buffer solution (0.1 M, $Na_2HPO_4/NaHPO_4$, pH 7.0) was used as a supporting electrolyte due to its matching properties to those liquids' presence in the human body. Current-voltage (*I-U*) sweeps were recorded from -2 V to 2 V after adding aliquots of *D*- glucose, freshly prepared on the day of the experiment. Hence, a calibration curve was obtained by adding aliquots of a standard solution while performing *I-U* sweeps. All chemicals (*D*-$C_6H_{12}O_6$, $Na_2HPO_4/NaHPO_4$) were used as acquired (Merck, Germany) without any further purification. Standard solutions were prepared with ultrapure water (Arium mini, Sartorius, 18 MΩ cm).

Microscopic and spectroscopic analysis

The samples with memristive devices were thinned by site-specific focused ion beam technique (FIB, Helios NanoLab 650i, FEI). The thin lamella was cut from a carefully chosen memristor sample and thinned by Ga ions until the final thickness was less than 100 nm at 30 kV with a Zeiss 1540-XB. The microstructure studies were performed by conventional TEM (a JEOL JEM-2200FS.) operating at 200 kV.

A Theta probe system (Thermo Scientific, UK) was applied for XPS measurements, while the system was controlled by the Avantage software package provided by the system manufacturer. The samples were analyzed with monochromatic Al Kα X-Ray radiation with an energy of 1486.6 eV. The radiation is focused into 400μm diameter spots. Survey spectra were acquired with a pass energy of 200 eV and a binding energy step of 1 eV. For the high-resolution spectra, a pass energy of 20 eV with an energy step of 0.05 eV was used. A dual flood gun was used for the charge compensation accumulated on the surface. The measured spectra were calibrated to the C 1s peak of the adventitious carbon, found to be at 285.0 eV.
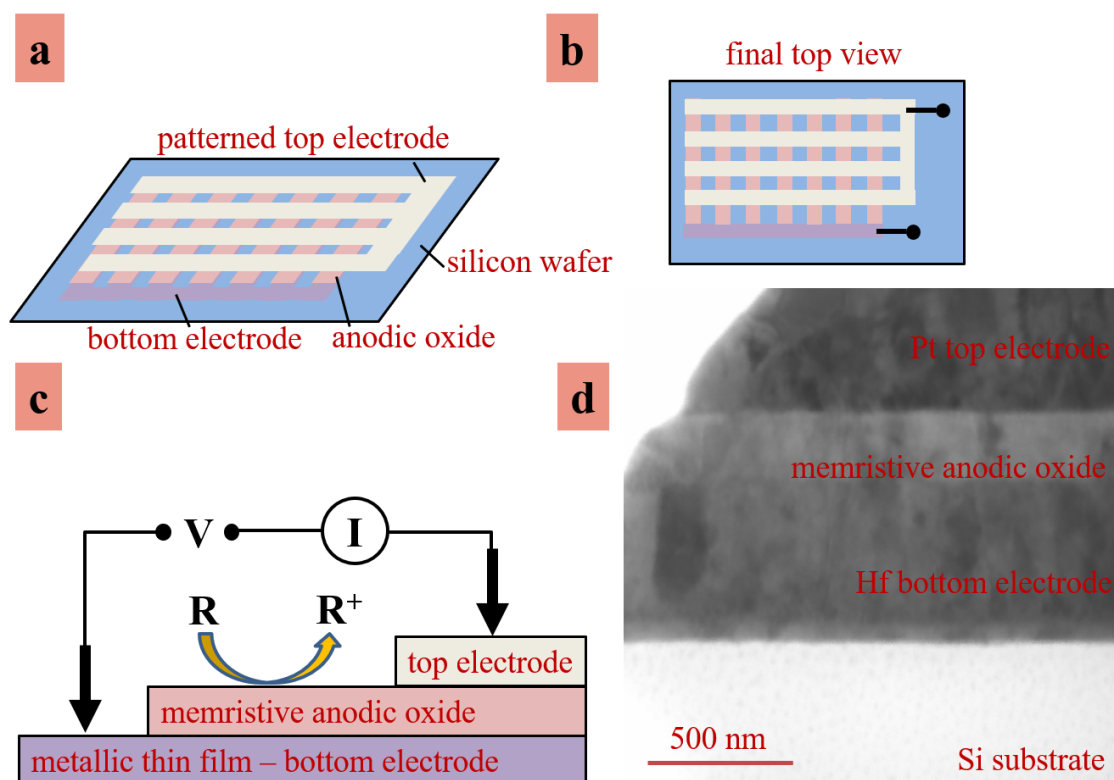
Figure 1. (a) Anodic memristors integrated in crossbar array. (b) A top view of anodic memristors integrated in crossbar array. (c) A single memristive sensor device. (d) Cross section of memristive sensor formed on Hf thin flims imaged by TEM

Results and discussion

Resistive switching of HfO₂ memristor sensors

The switching behavior of MIM structured devices (Figure 1c) has been studied by performing *I-U* sweeps. The structures, assembled at the intersections of metallic lines (Figure 1b), demonstrated typical bipolar memristive switching from -2 V to 2 V, as exemplified in Figure 2a (black *I-U* curve). The switching was observed at several resistive levels tested by applying different current limitation ranges during the voltage sweeping. This behavior was already observed for anodic memristors grown on Hf thin films in previous studies [35,36].

Once the switching effect was confirmed, a sensing response of memristors was investigated by drop-casting *D*-glucose at the surface of the device while performing *I-U* sweeps. The sensing analysis is based on the resistive state ratio extracted from *I-U* sweeps. This is schematically described in Figure 2a. Hence, HRS and LRS were extracted for a selected reading voltage. As it can be seen in Figure 2a, the resistive state ratio was lower for the *I-U* curve obtained by sweeping voltage without an analyte. By adding *D*-glucose, the resistive state ratio increased dramatically (Figure 2a, red *I-U* curve). This demonstrates the sensing capabilities of the device, which are most likely linked to the dynamics of the accumulation zones beneath the top electrode [38]. Electrolyte species containing hydroxyl groups diffuse on the surface and influence the position and size of these zones, directly influencing the redox cycle of the CFs during switching [36].

Following that, a quantification of glucose was studied by selecting four different concentrations (10, 20, 40 and 80 mM of *D* - glucose) to be drop cast at the surface of the sensor. In this case, typical *I-U* measurements were performed for each selected concentration one after the other (Figure 2b). The slopes of *I-U* curves, recorded for different *D*-glucose concentrations, changed as illustrated in

Figure 2b. It was observed that the resistive state ratios increased with the concentration of *D*-glucose (Figure 2). As noticed, the shape of *I-U* curves recorded for memristor sensors was mainly irregular. On the one hand, the respective curves of *I-U* sweeps recorded without the addition of standard solution exhibited a symmetric hysteresis loop (Figure 2a, black curve), switching bipolarly in both positive and negative voltage values range. On the other hand, the regular switching trend was demonstrated only in the positive voltage range for *I-U* sweeps recorded for the memristor sensor with the addition of the *D*-glucose standard solution. The resistive state ratio in negative voltage switching range values was significantly lower (Figure 2b). Hence, only the resistive switching in the positive voltage values range was considered for the calibration curve.

However, the *I-U* sweeps recorded for a number of memristors (5 up to 25 selected devices) demonstrated variations of device resistance values (considering both LRS and HRS values). Accordingly, the resistive state ratios ranged from 10 up to a few orders of magnitude.

Once the sensing response was proven, the possibility of quantifying *D*-glucose was tested for all devices, showing either a low resistive state ratio or a high resistive state ratio. Devices, which reached the resistive state ratio in the range of a few orders of magnitude, did not show a linear trend in resistive state ratio change with respect to added *D*-glucose concentration (Figure 2c). Hence, the sensing capabilities in the case of higher resistive state ratios were lower as compared to lower ratios, as explained further. Increasing the concentration of glucose exponentially increased the current response.

In other words, LRS values decreased while the resistive state ratio increased. Eventually, memristors were irreversibly switched due to dielectric breakdown or possible permanent conductive filaments (CFs) disruption. It may be assumed that the stability of CFs, formed inside the active oxide, directly affects the performance of sensors [18,20,39]. Therefore, there is a strong motivation to use the anodic HfO_2 memristor concept for sensing applications assuming the stability of CFs. An improved switching performance of HfO_2 memristors is explained by CFs pinning, which was confirmed for HfO_2 grown in phosphate buffer [18].

The resistive state ratio increased linearly with respect to four different *D*-glucose concentrations for memristive devices that initially reached a resistive state ratio in the range of several ohms (Figure 2b). This proves higher sensing capabilities in the case of lower resistive state ratios. This was already linked to CFs stability. Permanent destruction of CFs is immediate for higher initial resistive state ratios due to higher current passing through in the low state. For this reason, these MIM structures were considered for further optimization of experimental parameters.
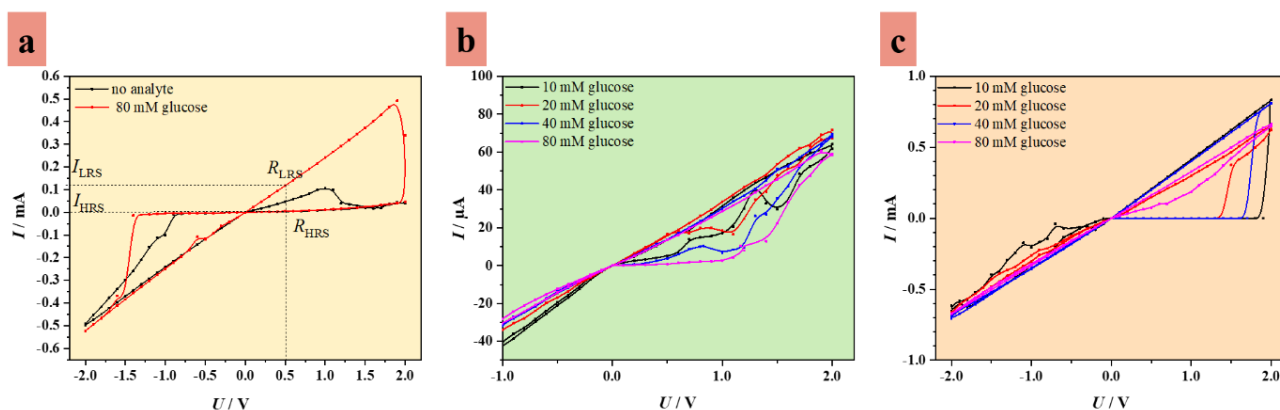
Figure 2. *(a) I-U sweeps recorded for memristor without analyte and (b) with the addition of D-glucose. (c) dependence of I-U sweeping response on the concentration of D-glucose (10 to 80 mM)*

Analytical performance of anodic HfO$_2$ memristor sensor

The analytical performance of sensors was studied based on at least five different devices that have shown stable switching voltage range from -2 to 2 V. During the voltage sweeping, the current limitation was set to a maximum of 1 mA. The resistive switching was observed in the low current range, reaching up to 100 µA. Four different D-glucose concentrations were selected for quantification. As already described, *I-U* sweeps were recorded for each selected concentration (10, 20, 40 and 80 mM of D-glucose). Resistive state ratio (HRS/LRS) values were extracted from these curves and shown with respect to reading voltage values (Figure 3a). In order to avoid any possible error, HRS/LRS ratio values were determined by extracting LRS or HRS values always at the same reading voltage value. Figure 3b and 3c present a calibration curve obtained by extracting HRS/LRS ratios from *R-U* sweeps with respect to *D*-glucose concentrations. In this case, resistive state ratio values were extracted by reading LRS and HRS values at a selected reading voltage value of 20 mV. Additionally, resistive state ratio values for selected reading values, in the range from 0 to 2 V, are shown in Figure 3d. Error bars, shown in Figure 3d, are determined empirically by the variations in extracted HRS/LRS values between different devices.
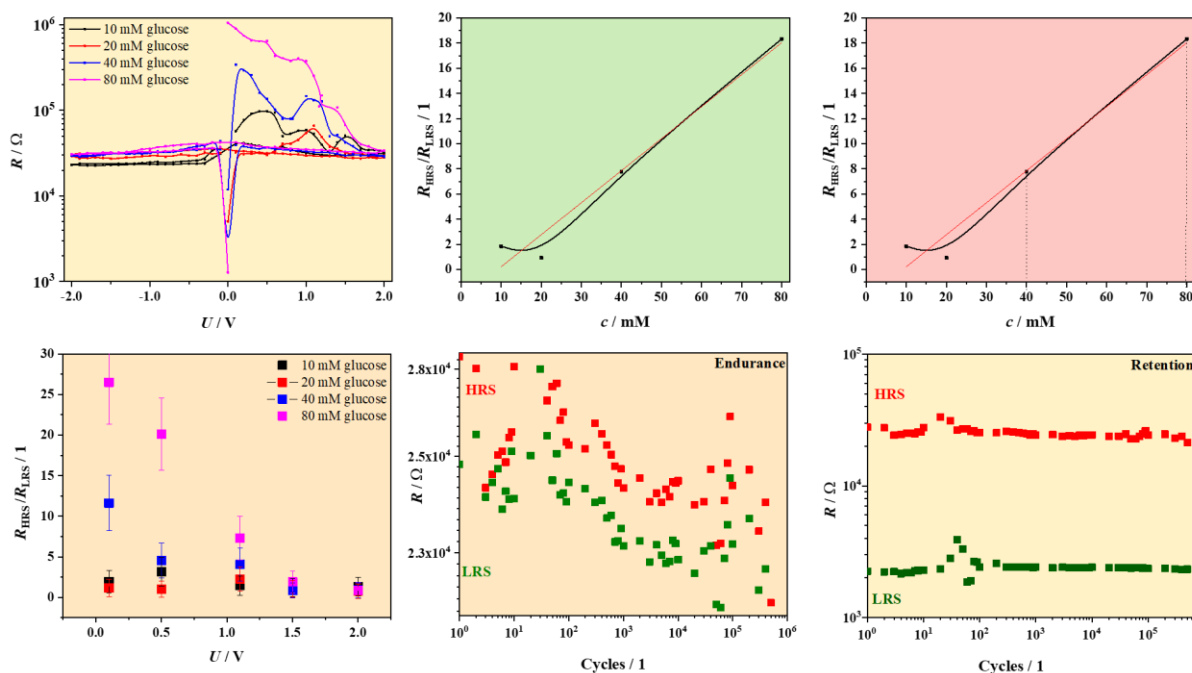
***Figure 3**. (a) R-U sweeps extracted for different D-glucose concentrations. (b), (c) Calibration curve obtained in 0.1 M phosphate buffer for 10 Mm -80 mM D-glucose. (d) Resistive state ratios extracted from I-U sweeps with respect to different reading voltage values. (e) Endurance assessment based on successive resistive switching. (f) Retention assessment based on successive resistive readings*

Linearity was found in the range from 10 mM to 80 mM with a corresponding correlation factor equal to $R^2 = 0.96809$. Moreover, the limit of detection (LOD) and limit of quantification (LOQ) were determined based on five different calibration curves using the lowest concentration of *D*-glucose. While LOD was estimated as 0.8 mM, LOQ was assessed as 2.6 mM. These LOD and LOQ values are relatively high compared to the values of conventional sensors reported in the literature. However, the determination of analytical parameters was not reported for HfO$_2$ anodic memristor-based sensors used for liquid detection. Only several liquid sensors using this concept, mainly based on TiO$_2$, have been communicated until now [6,31,40]. Hence, this work evidences an improved performance of such sensors regarding resistive state ratio but also enhanced quantification

possibilities. The development of memristive sensors integrated into crossbar arrays is relevant since a high number of devices can be studied at the same time. This is crucial for understanding the fundamental concept of miniaturized in-memory computing systems, possibly leading to their industrial implementation [7].

Moreover, the reproducibility based on five different sensors was evaluated as 3.7 %, while repeatability was estimated as 2.3 % for five measured HRS/LRS values using the same device. This confirms the high repeatability and stability of MIM structures, with no significant difference in HRS/LRS ratio recorded even if devices were used after a longer time. The extraction of analytical performance parameters is highly relevant for comparison, hence the future development of memristive sensors grown on different materials or in different geometry. For this reason, the sensitivity (S) of sensors was also evaluated by selecting two HRS/LRS ratio values from the calibration curve, for the corresponding concentrations (Figure 3c, equation (1)).

$$S = \frac{\dfrac{HRS_2}{LRS_2} - \dfrac{HRS_1}{LRS_1}}{c_2 - c_1} \tag{1}$$

The sensitivity was calculated as 5.3 mM^{-1}, thus being higher as compared to TiO$_2$-based memristive sensors produced by sputtering [6].

Finally, endurance and retention measurements were performed in order to confirm the stability of each sensor. This was done by successive resistive switching (followed by resistance evaluation) and successive resistive readings, respectively, and the results are presented in Figures 3e and 3f. The device lifetime and data retention reached up to 10^5 cycles. A high resistive state suddenly becoming conductive is the event that is considered the end of the lifetime or data retention. This is comparable to previously reported Hf-based anodic memristors [35,36].

XPS analysis

The composition of the oxide grown on Hf thin films was examined by XPS (Figure 4). The sample taken for the XPS analysis was drop cast with *D*-glucose and used as a MIM structured memristive sensor. The samples analyzed were covered by Pt top electrodes (as used for sensing purposes). In addition, depth profiling was performed to study the electrolyte species and glucose incorporation. In such a case, Pt was sputtered away. The presence of C, O, Hf and Pt was found at the surface of the anodic oxide grown in PB covered by Pt top electrode (Figure 4a-4d). Four chemical forms of C can be identified from C 1s high-resolution spectra (Figure 4b). The peak at 285.0 eV corresponds to adventitious C related to the C–C/C–H carbon type. The second peak found at 289.2 eV can be assigned to a carboxylic functional group (O═C–O), whereas the peak at 286.5 eV (C-O/N) is most likely related to the rest of glucose as C-OH reacting with impurities found within the sample being also present as amine at 399.4 eV (N 1s) [41,42]. The impurities found at the surface by depth profiling were less than 1 at.%, reaching 1.4 at.%. Oppositely, the peak at 288 eV (Figure 4b) is related to carbon bonded with a single covalent bond to oxygen (O-C-O) [41,42]. This points towards glucose penetrating the oxide/electrode interface, confirming the sensing concept stated in previous sections [41,42]. Moreover, two chemical forms of O can be noted based on the O 1s spectrum (Figure 4d). These peaks (Figure 4a and 4d) found at 532.8 and 531.3 eV are related to O from organic molecules (*D*-glucose) and O bound in oxides as HfO$_2$, respectively [41-43]. The electrolyte species incorporation in anodic oxide can be recognized only as a presence of Na$^+$ (Na 1s) at 1071.7 eV (Figure 4a). The stoichiometric amount of O to Hf within the same oxide is confirmed by a Hf 4f$_{7/2}$ peak at 16.9 eV and a Hf 4f$_{5/2}$ peak at 18.6 eV, representing HfO$_2$. A single chemical form of Hf (Figure 4c) is

visible in Figure 4d as Hf 4f scan [41-43]. Finally, the Pt top electrode above the oxides is recognized as Pt $4f_{5/2}$ and Pt $4f_{7/2}$ doublet (Figure 4a) at 73.9 and 70.6 eV, respectively [41-43]. Hence, the sensing capabilities of Hf memristive sensor are based on O species originating from *D*-glucose functional groups. Likely, O species penetrating the electrode/oxide are contributing to the event of CFs formation. This is achieved by their movement throughout the oxide induced by applying an external electric field. This results in resistive state ratio value change upon adding the analyte solution, as previously discussed.
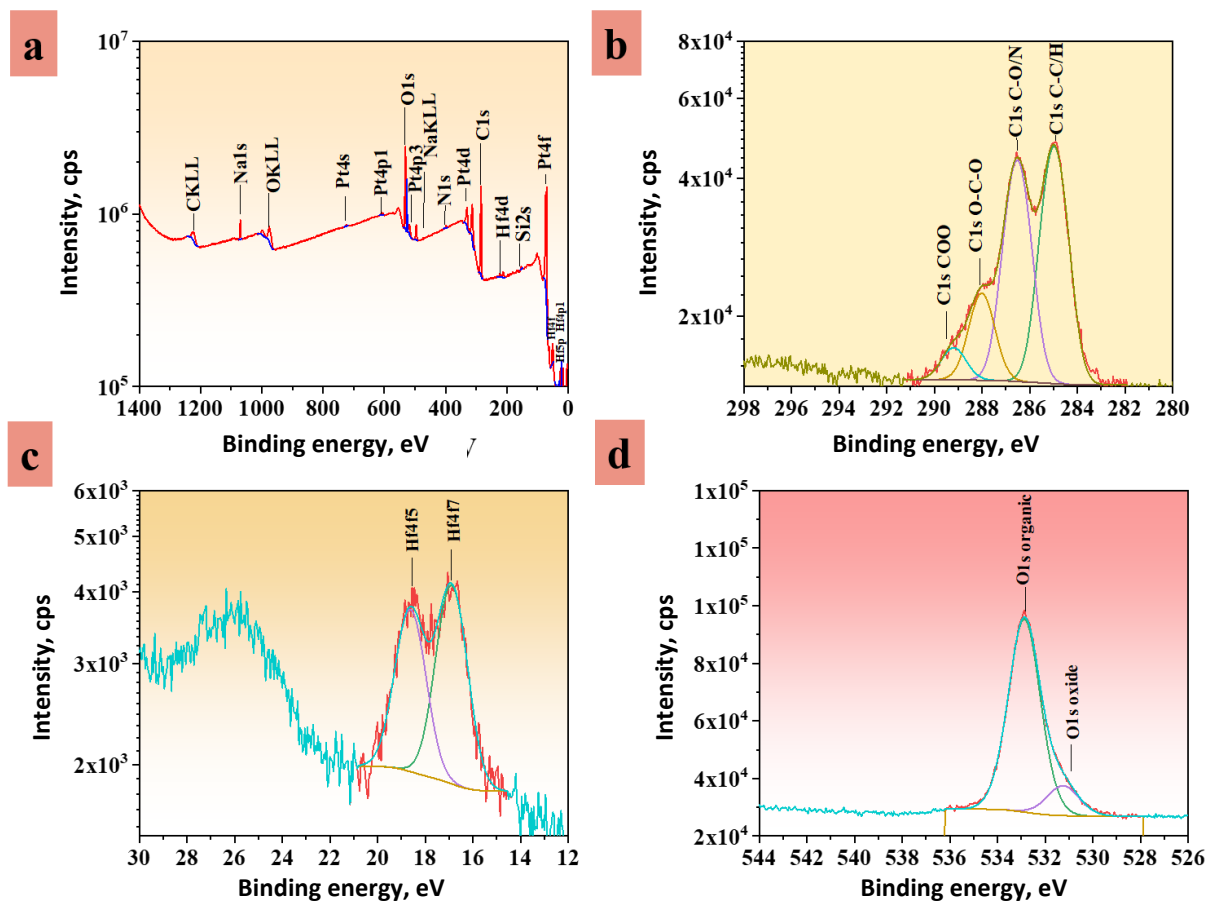
Figure 4. *a) XPS survey and b–d) high-resolution spectra of Hf memristive sensor samples prepared in phosphate buffer*

Conclusions

This study proves the concept of a memristive sensor based on hydroxyl group influence on accumulation regions in the vicinity of the top electrode. The sensing mechanism relying on resistive state ratio has been proven as a tool for qualitative and quantitative liquid detection. However, further optimization of the sensor is vital. The performance of such devices is dependent on the size of electrodes, the reliability of the pattering mask or the scan rate applied during *I-U* sweeps performance. Once the performance of each device is established, this will allow its functioning in a crossbar array, which is currently under study. Additionally, a standard solution of *D*-glucose was selected due to -OH groups in its structure, thus allowing further investigation of OH-contained liquids. This is important for the investigation of the selectivity of the sensor, possibly leading to real sample analysis and implementation of memristor sensors in biomedical applications, consequently.

Conflicts of Interest: *The authors declare no conflict of interest.*

References

[1] I. H. Im, S. J. Kim, H. W. Jang, Memristive Devices for New Computing Paradigms, *Advanced Intelligent Systems* **2** (2020) 2000105. https://doi.org/10.1002/aisy.202000105

[2] S. Carrara, The Birth of a New Field: Memristive Sensors. A Review, *IEEE Sensors Journal* **21** (2021) 12370-12378. https://doi.org/10.1109/JSEN.2020.3043305

[3] K. Sun, J. Chen, X. Yan, The Future of Memristors: Materials Engineering and Neural Networks, *Advanced Functional Materials* **31** (2021) 2006773. https://doi.org/10.1002/adfm.202006773

[4] A. Sebastian, M. Le Gallo, R. Khaddam-Aljameh, E. Eleftheriou, Memory devices and applications for in-memory computing, *Nature Nanotechnology* **15** (2020) 529-544. https://doi.org/10.1038/s41565-020-0655-z

[5] X. Zhang, A. Huang, Q. Hu, Z. Xiao, P.K. Chu, Neuromorphic Computing with Memristor Crossbar, *Physica Status Solidi A* **215** (2018) 1700875. https://doi.org/10.1002/pssa.201700875

[6] N.S. Mohamad Hadis, A. Abd Manaf, S. H. Ngalim, S.H. Herman, Fabrication and characterisation of fluidic based memristor sensor for liquid with hydroxyl group, *Sensing and Bio-Sensing Research* **14** (2017) 21-29. https://doi.org/10.1016/j.sbsr.2017.04.002

[7] Y. Meng, J. Zhu, Low energy consumption fiber-type memristor array with integrated sensing-memory, *Nanoscale Advances* **4** (2022) 1098-1104. https://doi.org/10.1039/d1na00703c

[8] Y. Zhou, Y. Li, L. Xu, S. Zhong, R. Xu, X. Miao, A hybrid memristor-CMOS XOR gate for nonvolatile logic computation, *Physica Status Solidi A* **213** (2016) 1050-1054. https://doi.org/10.1002/pssa.201532872

[9] G. W. Burr, R. M. Shelby, A. Sebastian, S. Kim, S. Kim, S. Sidler, K. Virwani, M. Ishii, P. Narayanan, A. Fumarola, L. L. Sanches, I. Boybat, M. Le Gallo, K. Moon, J. Woo, H. Hwang, Y. Leblebici, Neuromorphic computing using nonvolatile memory, *Advances in Physics: X* **2** (2017) 89-124. https://doi.org/10.1080/23746149.2016.1259585

[10] A. Irmanova, A.P. James, Multi-level memristive memory with resistive networks, *Asia Pacific Conference on Postgraduate Research in Microelectronics & Electronics*, Kuala Lumpur, Malaysia, 31 October - 2 November 2017, 69-72. https://doi.org/10.1109/PRIMEASIA.2017.8280366

[11] T. Y. Wang, J. L. Meng, Q. X. Li, Z.Y. He, H. Zhu, L. Ji, Q. Q. Sun, L. Chen, D. W. Zhang, Reconfigurable optoelectronic memristor for in-sensor computing applications, *Nano Energy* **89** (2021) 106291. https://doi.org/10.1016/j.nanoen.2021.106291

[12] B. Mohammad, M.A. Jaoude, V. Kumar, D.M. Al Homouz, H.A. Nahla, M. Al-Qutayri, N. Christoforou, State of the art of metal oxide memristor devices, *Nanotechnology Reviews* **5** (2016) 311-329. https://doi.org/10.1515/ntrev-2015-0029

[13] A. K. Parit, M. S. Yadav, A. K. Gupta, A. Mikhaylov, B. Rawat, Design and modeling of niobium oxide-tantalum oxide based self-selective memristor for large-scale crossbar memory, *Chaos, Solitons and Fractals* **145** (2021) 110818. https://doi.org/10.1016/j.chaos.2021.110818

[14] L. Shi, G. Zheng, B. Tian, B. Dkhil, C. Duan, Research progress on solutions to the sneak path issue in memristor crossbar arrays, *Nanoscale Advances* **2** (2020) 1811-1827. https://doi.org/10.1039/d0na00100g

[15] S. Choi, S. Jang, J. H. Moon, J. C. Kim, H. Y. Jeong, P. Jang, K. J. Lee, G. Wang, A self-rectifying TaOy/nanoporous TaOx memristor synaptic array for learning and energy-efficient neuromorphic systems, *NPG Asia Materials* **10** (2018) 1097-1106. https://doi.org/10.1038/s41427-018-0101-y

[16] S. Dirkmann, J. Kaiser, C. Wenger, T. Mussenbrock, Filament Growth and Resistive Switching in Hafnium Oxide Memristive Devices, *ACS Applied Materials & Interfaces* **10** (2018) 14857-14868. https://doi.org/10.1021/acsami.7b19836

[17] T. Mikolajick, H. Wylezich, H. Maehne, S. Slesazeck, Versatile resistive switching in niobium oxide, *Proceedings - IEEE International Symposium on Circuits and Systems,* Montreal, QC, Canada, 22-25 May 2016, 381-384. https://doi.org/10.1109/ISCAS.2016.7527250

[18] I. Zrinski, C. C. Mardare, L.-I. Jinga, J. P. Kollender, G. Socol, A. W. Hassel, A. I. Mardare, Phosphate incorporation in anodic hafnium oxide memristors, *Applied Surface Science* **548** (2021) 149093. https://doi.org/10.1016/j.apsusc.2021.149093

[19] H. Abunahla, M. A. Jaoude, C. J. O'Kelly, Y. Halawani, M. Al-Qutayri, S. F. Al-Sarawi, B. Mohammad, Switching characteristics of microscale unipolar Pd/Hf/HfO2/Pd memristors, *Microelectronic Engeering* **185**–**186** (2018) 35-42. https://doi.org/10.1016/j.mee.2017.10.010

[20] I. Zrinski, A. Minenkov, C. Cancellieri, R. Hauert, C. C. Mardare, J. P. Kollender, L. P. H. Jeurgens, H. Groiss, A. W. Hassel, A. I. Mardare, Mixed anodic oxides for forming-free memristors revealed by combinatorial screening of hafnium-tantalum system, *Applied Materials Today* **26** (2022) 101270. https://doi.org/10.1016/j.apmt.2021.101270

[21] S. Saylan, M. A. Jaoude, K. Humood, F. Ravaux, H. F. A. Shehhi, B. Mohammad, Silver/(sub-10 nm)hafnium-oxide-based resistive switching devices on silicon: Characteristics and switching mechanism, *Nanotechnology* **31** (2020) 165202. https://doi.org/10.1088/1361-6528/ab68fb

[22] S. Chen, S. Noori, M. A. Villena, Y. Shi, T. Han, Y. Zuo, M. P. Pedeferri, D. Strukov, M. Lanza, M.V. Diamanti, Memristive electronic synapses made by anodic oxidation, *Chemistry of Materials* **31** (2019) 8394-8401. https://doi.org/10.1021/acs.chemmater.9b02245

[23] S. M. Edlou, A. Smajkiewicz, G. A. Al-Jumaily, Optical properties and environmental stability of oxide coatings deposited by reactive sputtering, *Applied Optics* **32** (1993) 5601. https://doi.org/10.1364/ao.32.005601

[24] P. S. Lysaght, B. Foran, G. Bersuker, P. J. Chen, R. W. Murto, H.R. Huff, Physicochemical properties of HfO2 in response to rapid thermal anneal, *Applied Physics Letters* **82** (2003) 1266-1268. https://doi.org/10.1063/1.1553998

[25] P. Baumeister, O. Arnon, Use of hafnium dioxide in multilayer dielectric reflectors for the near uv, *Applied Optics* **16** (1977) 439. https://doi.org/10.1364/ao.16.000439

[26] M. Gilo, N. Croitoru, Study of HfO₂ films prepared by ion-assisted deposition using a gridless end-hall ion source, *Thin Solid Films* **350** (1999) 203-208. https://doi.org/10.1016/S0040-6090(99)00226-6

[27] D. Reicher, P. Black, K. Jungling, Defect formation in hafnium dioxide thin films, *Applied Optics* **39** (2000) 1589. https://doi.org/10.1364/ao.39.001589

[28] J. Lu, Y. Kuo, J.-Y. Tewg, Hafnium-Doped Tantalum Oxide High-k Gate Dielectrics, *Journal of The Electrochemical Society* **153** (2006) G410 https://doi.org/10.1149/1.2180647

[29] J. L. Courouau, J. Fouletier, M. C. Steil, HfO₂-based electrolyte potentiometric oxygen sensors for liquid sodium, *Electrochimica Acta* **331** (2020) 135269. https://doi.org/10.1016/j.electacta.2019.135269

[30] V. Dave, P. K. Mishra, R. Chandra, Nanostructured Hafnium Oxide Thin films for Sensing Carbon Monoxide: An Experimental Investigation, *Materials Today: Proceedings* **5** (2018) 23286-23292. https://doi.org/10.1016/j.matpr.2018.11.062

[31] N. S. M. Hadis, A. A. Manaf, S. H. Herman, S. H. Ngalim, High Roff/Ron ratio liquid based memristor sensor using sol gel spin coating technique, *Proceedings of IEEE Sensors,* Busan, Korea,1-4 November 2015. https://doi.org/10.1109/ICSENS.2015.7370379

[32] X. Bi, C. Zhang, H. Li, Y. Chen, R. E. Pino, Spintronic memristor based temperature sensor design with CMOS current reference, 2012 *Design, Automation & Test in Europe Conference & Exhibition (DATE),* Dreseden, Germany, 12-16 March 2012, 1301-1306. https://doi.org/10.1109/date.2012.6176693

[33]   S. Carrara, D. Sacchetto, M. A. Doucey, C. Baj-Rossi, G. De Micheli, Y. Leblebici, Memristive-biosensors: A new detection method by using nanofabricated memristors, S*ensors and Actuators B* **171**-**172** (2012) 449-457. https://doi.org/10.1016/j.snb.2012.04.089

[34]   F. Puppo, M. A. Doucey, M. Di Ventra, G. De Micheli, S. Carrara, Memristor-based devices for sensing, *IEEE International Symposium on Circuits and Systems (ISCAS),* Melbourne, Victoria, Australia, 1-5 June 2014, 2257-2260. https://doi.org/10.1109/ISCAS.2014.6865620

[35]   I. Zrinski, C. C. Mardare, L.-I. Jinga, J. P. Kollender, G. Socol, A. W. Hassel, A. I. Mardare, Phosphate incorporation in anodic hafnium oxide memristors, *Applied Surface Science* **548** (2021) 149093. https://doi.org/10.1016/j.apsusc.2021.149093

[36]   I. Zrinski, C. C. Mardare, L. I. Jinga, J. P. Kollender, G. Socol, A. Minenkov, A. W. Hassel, A. I. Mardare, Electrolyte - Dependent Modification of Resistive Switching in Anodic Hafnia, *Nanomaterials* **11(3)** (2021) 666. https://doi.org/10.3390/nano11030666

[37]   Sodium phosphate, *Cold Spring Harbor Protocols,* 2006. https://doi.org/10.1101/pdb.rec8303

[38]   G. S. Kim, T. H. Park, H. J. Kim, T. J. Ha, W. Y. Park, S. G. Kim, C. S. Hwang, Investigation of the retention performance of an ultra-thin HfO_2 resistance switching layer in an integrated memory device, *Journal of Applied Physics* **124** (2018) 024102. https://doi.org/10.1063/1.5033967

[39]   I. Zrinski, M. Löfler, J. Zavašnik, C. Cancellieri, L. P. H. Jeurgens, A. W. Hassel, A. I. Mardare, Impact of Electrolyte Incorporation in Anodized Niobium on Its Resistive Switching, *Nanomaterials* **12** (2022) 813. https://doi.org/10.3390/nano12050813

[40]   N. S. M. Hadis, A. A. Manaf, S. H. Herman, Characterization of ROFF/RON ratio of fluidic based memristor sensor for pH detection, *2015 IEEE Regional Symposium on Micro and Nanoelectronics,* Kuala Terengganu, Malaysia*,* 19-21 August 2015*.* https://doi.org/10.1109/RSM.2015.7354956

[41]   G. Beamson, D. Briggs, An International Journal at the Interface Between Chemistry and Physics High resolution monochromated X-ray photoelectron spectroscopy of organic polymers: A comparison between solid state data for organic polymers and gas phase data, *Molecular Physics* **75(4)** (1992) 37-41. https://doi.org/10.1080/00268979200101761-

[42]   D. Briggs, X-ray photoelectron spectroscopy (XPS), *Handbook of Adhesion, Second Edition* (2005) 621-622 https://doi.org/10.1002/0470014229.ch22

[43]   D. Barreca, A. Milanov, R. A. Fischer, A. Devi, E. Tondello, Hafnium oxide thin film grown by ALD: An XPS study, *Surface Science Spectra* **14** (2007) 34-40. https://doi.org/10.1116/11.20080401